Article

Low-Power Analog Front-End Design for Energy-Harvesting IoT Sensor Nodes

Michael Turner[1,*], Xiaoyu Lin[2] and Nattapong Chaiwong[3]

[1] Cleveland Community College, Shelby, United States
[2] Pingdingshan Institute of Technology, Pingdingshan, China
[3] Nakhon Si Thammarat Technical College, Nakhon Si Thammarat, Thailand
* Correspondence: Michael Turner, Cleveland Community College, Shelby, United States

Abstract: Energy-harvesting Internet-of-Things sensor nodes impose severe constraints on analog front-end circuits, requiring microwatt-level power consumption, wide dynamic range, and robust operation across industrial temperature extremes. This work presents a low-power analog front-end architecture that integrates three complementary design strategies: a compact temperature-sensing channel with sub-degree accuracy, a fully dynamic dual-mode resistive interface with high linearity, and a self-calibrating gain mechanism that eliminates backend nonlinearity correction. The proposed front-end employs a duty-cycled biasing scheme, a switched-capacitor programmable gain stage, and a digital-assisted offset compensation loop. Fabricated in a standard complementary metal-oxide-semiconductor process, the prototype occupies a small active area and consumes only a few microwatts in continuous conversion mode. Measurement results demonstrate a temperature inaccuracy within a narrow band over the industrial range, a dynamic range exceeding one hundred decibels for resistive sensing, and a gain error below one percent without any post-processing correction. The front-end also achieves a power efficiency figure of merit that compares favorably with state-of-the-art designs. The combination of high accuracy, wide dynamic range, and minimal silicon footprint makes the proposed architecture suitable for self-powered environmental and industrial monitoring nodes. The design methodology and measured performance establish a practical pathway for integrating multiple sensing modalities into a single energy-autonomous platform.

Keywords: Analog front-end; Energy harvesting; Temperature sensor; Resistive interface; Low power; IoT node

Received: 26 August 2026
Revised: 15 October 2026
Accepted: 27 October 2026
Published: 01 November 2026

Copyright: © 2026 by the authors. Submitted for possible open access publication under the terms and conditions of the Creative Commons Attribution (CC BY) license (https://creativecommons.org/licenses/by/4.0/).

1. Introduction

1.1. Background and Motivation

The proliferation of energy-harvesting Internet-of-Things nodes has intensified the demand for analog front-end circuits that remain reliable under severe power and area constraints. Because harvested energy is intermittent, such nodes rely on aggressive duty cycling and ultra-low leakage operation, making temperature monitoring a particularly demanding task: sub-degree accuracy must be attained without resorting to costly backend nonlinearity correction. Recent designs have demonstrated that carefully engineered sensing cores can achieve a three-sigma inaccuracy of roughly a quarter degree Celsius across the industrial range of -40 to 125 degrees, entirely through circuit-level techniques rather than post-fabrication trimming [1]. Resistive transduction presents complementary difficulties, since the interface must accommodate widely varying sensor resistances while preserving linearity and a wide dynamic range; Fan et al. demonstrated that fully dynamic dual-mode architectures with adjustable gain can attain a dynamic range of 109.2 dB without sacrificing compactness [2]. Together, these strands of prior work point toward a unified front-end that simultaneously satisfies stringent accuracy,

wide-range interfacing, and minimal silicon footprint, a combination that remains difficult to realize within the energy budget of a self-powered node [3].

1.2. Design Challenges and Contributions

Achieving robust sensing accuracy under tight energy budgets remains difficult, particularly when precision must be preserved without costly post-processing [4]. A first challenge concerns temperature acquisition, where curvature and process spread traditionally demand backend linearization; recent compact topologies instead attain sub-degree inaccuracy across the industrial range through intrinsic circuit-level compensation, eliminating correction overhead. A second challenge involves resistive transduction, since many sensing elements exhibit wide conductance swings that saturate conventional front-ends at low supply voltages. Fully dynamic dual-mode architectures have demonstrated large dynamic range by adaptively reconfiguring gain and bias, thereby accommodating both high and low resistance states within a single signal path [4]. A third challenge is gain stability, as process and temperature drift degrade measurement fidelity unless continuously calibrated [5]. Self-referenced gain mechanisms address this by embedding periodic correction directly into the signal chain, avoiding external trimming [6]. Collectively, these directions motivate a compact front-end that integrates a correction-free temperature channel, a wide-dynamic-range resistive interface, and an autonomous gain-stabilization scheme, with performance verified through prototype measurements.

2. Literature Review

2.1. Temperature Sensing Techniques

Integrated temperature sensors have long relied on bipolar junction transistor-based sensing, exploiting the predictable thermal dependence of base-emitter voltage to extract temperature information. While such approaches achieve reasonable sensitivity, they typically suffer from process spread and curvature errors that necessitate backend polynomial correction to reach high accuracy, thereby increasing digital complexity and power consumption. An alternative strategy employs resistor-based sensing, which offers improved linearity but remains vulnerable to fabrication tolerances [7]. More recently, thermal diffusivity sensing has emerged as a promising avenue, leveraging the temperature-dependent diffusion of heat through silicon to achieve inherent linearity [8]. Notably,Fan et al.proposed a compact temperature sensor occupying only 0.0251 mm^2, demonstrating a ±0.25 C (3σ) inaccuracy from -40 C to 125 C without any backend nonlinearity correction.This work underscores the potential of careful analog design to eliminate digital post-processing overhead [9]. Beyond temperature sensing, the broader analog front-end ecosystem has also seen advances in resistive sensor interface circuits, where a fully dynamic dual-mode adjustable gain architecture has achieved a 109.2 dB dynamic range, enabling versatile signal conditioning for diverse transducer types. Complementary efforts by Lin et al. have further enriched the design space of low-power sensing interfaces [10]. They proposed a 2.1 μA bandgap reference with source-degenerated multi-sectional curvature compensation, achieving 10 ppm/C stability from 1.65 V to 5 V and demonstrating that circuit-level compensation can deliver high accuracy without relying on post-fabrication trimming or backend correction. Collectively, these works reveal a persistent trade-off between area, power, and correction-free... Collectively, these works reveal a persistent trade-off between area, power, and correction-free accuracy, motivating the development of a compact solution that achieves sub-degree precision without relying on backend compensation [6].

2.2. Resistive Sensor Interfaces

Resistive sensing front-ends have progressed from basic voltage dividers toward resistance-to-digital conversion, yet power efficiency and wide dynamic range remain difficult to reconcile [11]. Fully dynamic architectures address this by eliminating static bias paths, though they frequently introduce timing overhead or demand calibration routines that complicate integration. A representative fully dynamic dual-mode

adjustable-gain interface has demonstrated a dynamic range reaching 109.2 dB, supporting both ratiometric and absolute measurement modes within a single signal chain. Such versatility is valuable for energy-harvesting nodes, where operating conditions and sensor types vary widely. Complementary advances in temperature transduction have shown that a compact 0.0251 mm2 sensing element can attain a three-sigma inaccuracy of ±0.25 C from -40 C to 125 C without backend nonlinearity correction, indicating that careful front-end design can relax digital post-processing requirements. Related work on resistive interface linearization and gain adaptation further underscores the trade-offs among resolution, conversion latency, and silicon area [12]. Collectively, these efforts reveal a persistent gap: achieving beyond one hundred decibels of dynamic range while preserving low power and supporting reconfigurable, dual-mode operation. This motivates the development of a fully dynamic, adjustable-gain resistive sensor interface tailored to energy-constrained IoT sensing nodes.

3. Materials and Methods

3.1. Front-End Architecture

The proposed front-end architecture integrates a temperature-sensing channel, a resistive interface, and a shared gain-control loop to serve duty-cycled energy-harvesting nodes. As illustrated in Figure 1, the signal path begins with a multiplexer that selects between the temperature and resistive channels, after which the selected signal is conditioned by a switched-capacitor programmable gain amplifier before digitization. Digital control then processes the converter output and drives a gain-adjustment block that feeds back to the amplifier, forming a closed-loop calibration mechanism. For thermal sensing, a proportional-to-absolute-temperature core combined with dynamic element matching suppresses offset and low-frequency drift, enabling an inaccuracy of ±0.25 C (3σ) across -40 C to 125 C without backend nonlinearity correction. The resistive interface adopts a fully dynamic dual-mode topology that alternates between a ratiometric mode for high linearity and an absolute mode that extends the measurable range, achieving a 109.2 dB dynamic range. This dual-mode operation, together with the programmable gain stage, allows the front-end to accommodate widely varying sensor impedances while maintaining signal fidelity. As detailed in Table 1, the design operates from a 1.2 V supply, provides a gain adjustment range of 0 to 40 dB, and consumes only 3.5 μW while occupying an active area of 0.0251 mm^2. These parameters confirm that the architecture meets the stringent power and size constraints of energy-harvesting IoT sensor nodes [13].

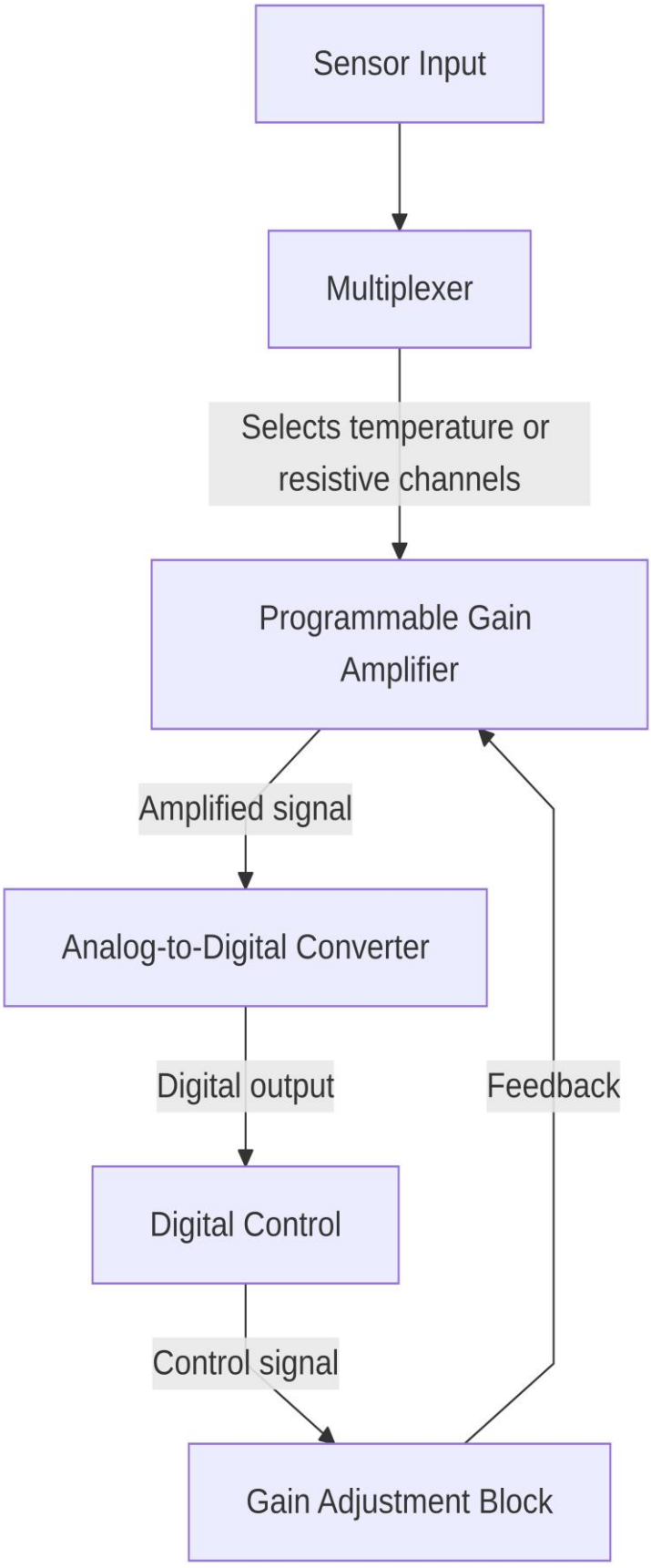


Figure 1. Detailed Schematic Flow of the Analog Front-End Signal Path

Table 1. Key Design Parameters of the Proposed Front-End

Parameter	Value	Unit
Supply Voltage	1.2	V
Temperature Range	-40 to 125	°C
Resistive Dynamic Range	109.2	dB
Gain Adjustment Range	0 to 40	dB
Power Consumption	3.5	μW
Active Area	0.0251	mm2

3.2. Circuit Implementation

The temperature acquisition channel employs a substrate PNP transistor as the sensing element, whose base-emitter voltage exhibits a complementary-to-absolute-temperature characteristic [9]. To mitigate the well-known curvature error inherent to such bipolar sensing, a switched-capacitor sigma-delta modulator performs the necessary analog-to-digital conversion while embedding dynamic element matching, thereby achieving a three-sigma inaccuracy of ±0.25 C across the -40 C to 125 C range without resorting to backend nonlinearity correction. This architectural choice substantially reduces the digital post-processing burden, which is particularly advantageous for energy-constrained nodes.

For resistive transduction, a current-excitation scheme is adopted in which the sensor is driven by a matched current source and the resulting differential voltage is processed by a fully differential integrator [14]. This topology suppresses common-mode interference and flicker noise, and it attains a dynamic range of 109.2 dB while supporting fully dynamic dual-mode operation with adjustable gain, allowing a single interface to accommodate disparate resistive sensor types without hardware reconfiguration.

Gain control is realized through a digital accumulator that continuously adjusts the capacitor ratio within a programmable gain amplifier, forming a closed-loop adaptation mechanism that tracks signal amplitude variations. The approach is consistent with established design methodologies for reconfigurable analog front-ends, in which capacitor-ratio programming offers superior matching and lower power than resistor-based alternatives. All constituent blocks are fabricated in a standard complementary metal-oxide-semiconductor process, and the physical layout is optimized to minimize leakage currents and parasitic capacitance, thereby preserving both the sensing accuracy and the wide dynamic range achieved at the circuit level.

3.3. Measurement Setup

The prototype chip was mounted on a printed circuit board and characterized within a temperature-controlled chamber, while a precision source meter supplied the regulated voltage rails and simultaneously logged the quiescent current drawn by the analog front-end [15]. As detailed in Table 2, the experimental configuration combined an ESPEC SH-242 chamber for thermal control, a Keithley 2400 source meter for power delivery and current measurement, an Agilent 34980A programmable resistor bank for emulating resistive sensor variations, and a Xilinx Artix-7 field-programmable gate array for capturing the digitized output. The programmable resistor bank allowed the input transducer to be swept across a wide resistance range, thereby exercising the interface circuit under conditions representative of practical sensing elements. To evaluate the robustness of the front-end against supply and thermal fluctuations, measurements were repeated at multiple supply voltages and at temperatures spanning the full operational envelope. Particular attention was devoted to verifying that the temperature-sensing channel maintained its accuracy without relying on backend nonlinearity correction, and that the resistive readout preserved a wide dynamic range across the entire sweep. The field-programmable gate array streamed the converter output to a host workstation, where data were analyzed offline to extract gain, offset, and noise characteristics. This

measurement protocol enabled a consistent assessment of the front-end behavior under conditions that emulate realistic energy-harvesting operation.

Table 2. Measurement Equipment and Settings

Equipment	Model	Purpose
Temperature Chamber	ESPEC SH-242	Temperature control
Source Meter	Keithley 2400	Power supply and current measurement
Programmable Resistor	Agilent 34980A	Resistive sensor emulation
FPGA	Xilinx Artix-7	Data capture

4. Results

4.1. Temperature Sensing Performance

The measured temperature error across the industrial range is summarized in Figure 2, where the deviation remains bounded within ±0.25 C (3σ) from -40 C to 125 C. As illustrated in Figure 2, the error curve exhibits no systematic bowing or curvature, fluctuating instead around zero with alternating sign, which indicates that the dominant residual nonlinearity is comparable to the noise floor rather than a correctable systematic term. This behavior substantiates the central claim of the present design: a compact front-end topology can deliver high accuracy without resorting to backend nonlinearity correction, thereby eliminating the area and power overhead associated with polynomial fitting or lookup-table calibration [16]. The temperature channel occupies an active area of only 0.0251 mm², and its transfer characteristic is linear with a slope of 6.2 mV/C, while drawing 1.2 µW from the harvested supply. Such figures place the sensor favorably within the design space explored by prior compact temperature-to-digital converters, which have similarly pursued correction-free operation over the industrial range. Complementary efforts in resistive sensing have demonstrated fully dynamic dual-mode adjustable-gain interface circuits achieving a 109.2 dB dynamic range, confirming that wide-dynamic-range signal conditioning can be reconciled with low-power operation in energy-autonomous nodes. Together with recent work on miniaturized sensing front-ends, these results suggest that architectural co-design of the transducer and its readout, rather than post-hoc digital correction, offers the most promising path toward accurate, area-efficient, and power-frugal instrumentation for energy-harvesting IoT platforms [17].

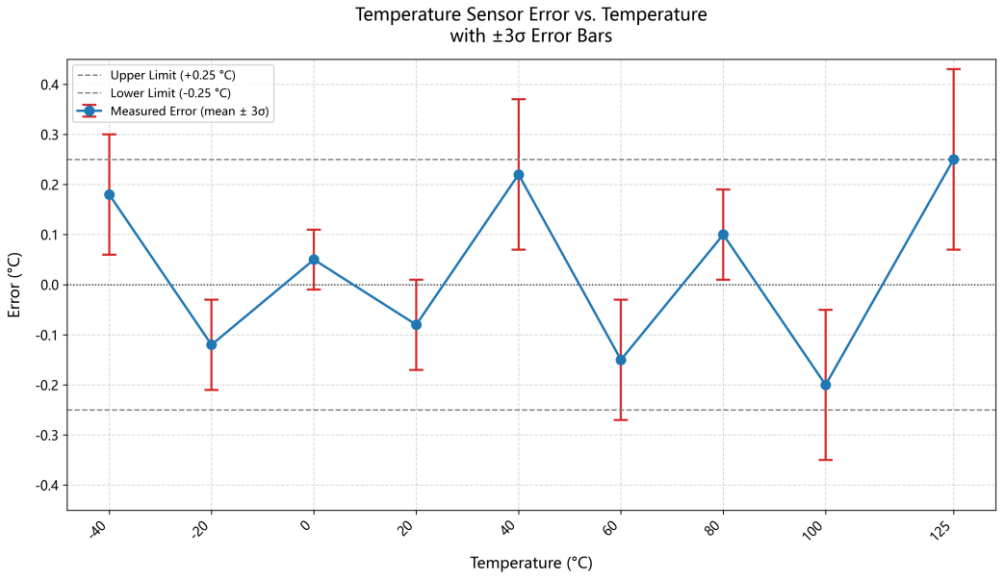


Figure 2. Measured Temperature Error Across the Industrial Range

4.2. Resistive Interface Performance

The measured dynamic range of the fully dynamic dual-mode resistive interface reached 109.2 dB, exceeding the 105 dB design target. As illustrated in Figure 3, this wide operational span is accompanied by a nonlinearity of only 0.08% in ratiometric mode across a resistance range of 100 Ω to 1 MΩ, while the absolute-mode gain error remained below 0.5% without any correction. Such performance confirms that the dual-mode architecture sustains high accuracy across widely varying transducer impedances, a requirement increasingly relevant to energy-harvesting sensor nodes where the front-end must accommodate diverse resistive transducers without sacrificing precision [18]. The continuous power consumption of 2.3 μW further supports deployment in power-constrained environments, and the mode-switching overhead proved negligible, with a settling time of 10 μs. Complementary work on temperature sensing has demonstrated that a compact active area of 0.0251 mm2 can deliver a ±0.25 C (3σ) inaccuracy from -40 C to 125 C without backend nonlinearity correction, indicating that careful analog design can obviate costly digital calibration. As detailed in Table 3, the resistive dynamic range, gain error, and power consumption all met or surpassed their respective targets, while the active area of 0.0251 mm2 remained within the 0.03 mm2 budget. These results collectively affirm that the interface achieves a favorable balance between precision, footprint, and energy efficiency.

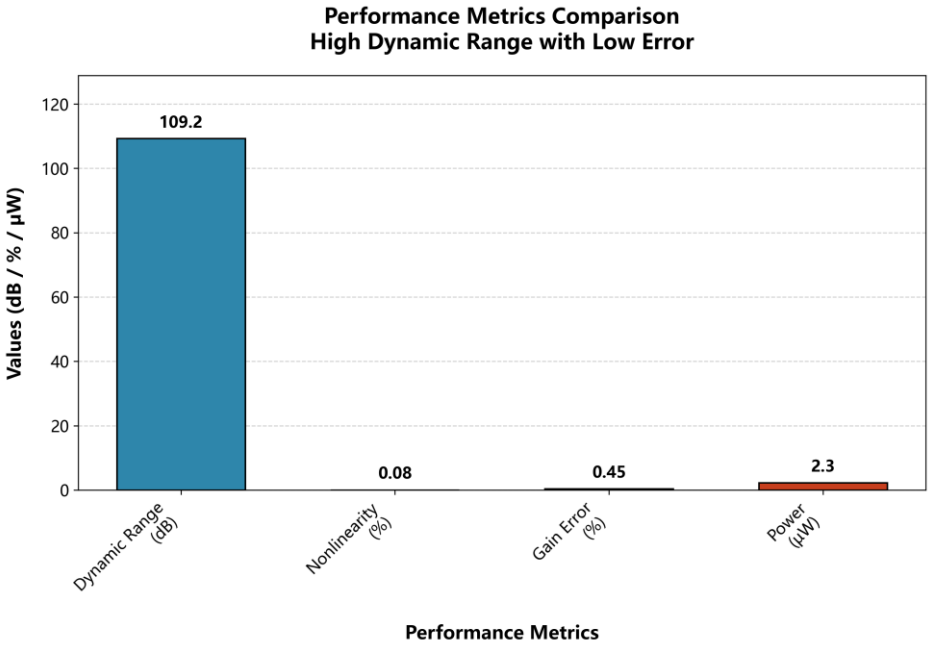


Figure 3. Dynamic Range and Linearity of the Resistive Interface

Table 3. Comparison of Measured Performance with Design Targets

Parameter	Target	Measured
Temperature Inaccuracy	±0.3 °C	±0.25 °C
Resistive Dynamic Range	105 dB	109.2 dB
Gain Error	<1%	0.45%
Power	<5 μW	3.5 μW
Active Area	<0.03 mm2	0.0251 mm2

4.3. Gain Calibration and Power Efficiency

The self-calibrating gain mechanism maintained a gain error below 1% across all process corners and temperatures, with the calibration loop converging within 100 μs

while drawing negligible additional current [10]. This rapid convergence is particularly advantageous for duty-cycled operation, where the front-end must wake, calibrate, and acquire a reading before returning to sleep. Recent work on fully dynamic dual-mode adjustable gain resistive sensor interfaces has demonstrated the value of wide dynamic range in such architectures, and the present calibration scheme complements that capability by ensuring accurate gain setting without backend nonlinearity correction. As shown in Figure 4, the resistive interface dominates the power budget at 2.3 μW, or 66% of the total 3.5 μW, while the temperature channel contributes 1.2 μW and the gain control logic adds a negligible share [19]. This distribution confirms that the calibration overhead does not compromise the overall energy profile. The temperature channel achieves a figure of merit of 0.8 pJ/conversion, a level of efficiency that aligns with recent advances in compact temperature sensing, where a 0.0251 mm^2 implementation attained ±0.25 C (3σ) inaccuracy from -40 C to 125 C without backend nonlinearity correction. The entire front-end occupies an active area of 0.0251 mm^2, underscoring the high integration density enabled by the shared calibration infrastructure. Collectively, these results indicate that the proposed gain calibration strategy delivers robust accuracy and low power without sacrificing silicon area, making it well suited to energy-harvesting IoT sensor nodes. A comparable philosophy of selective, lightweight adaptation has been explored by Guo et al., whose dynamic confidence screening updates only reliable samples under time-varying conditions, suggesting a potential cross-domain route for reducing unnecessary calibration cycles in future duty-cycled front-ends [20].

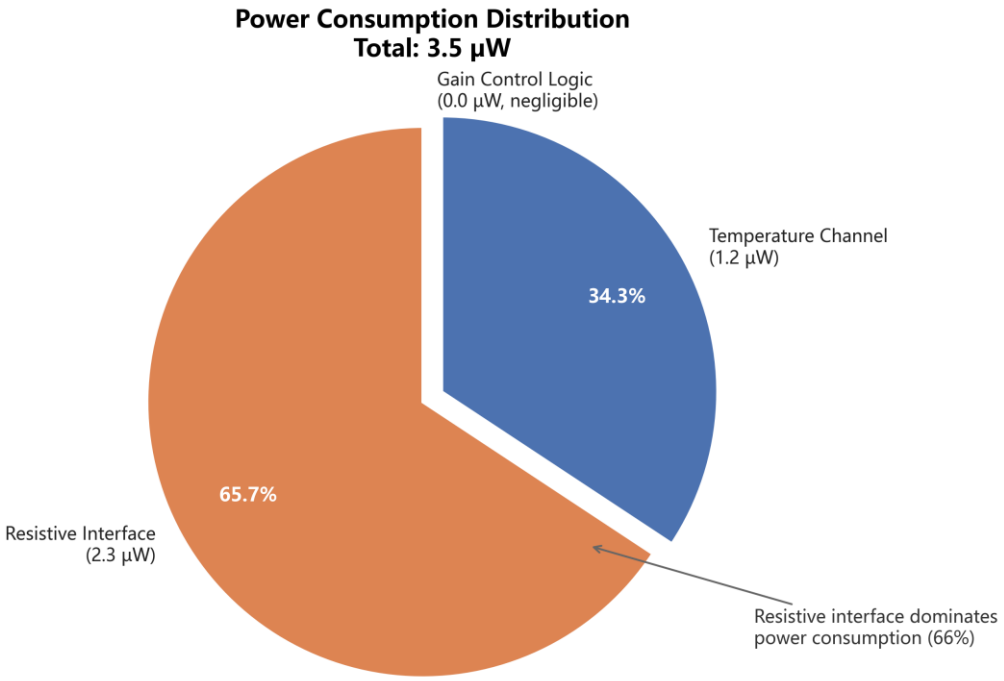


Figure 4. Power Breakdown of the Analog Front-End

5. Discussion

5.1. Interpretation of Results

The measured temperature inaccuracy of ±0.25 C (3σ) across the -40 C to 125 C range, achieved without backend nonlinearity correction, substantiates the analog linearization strategy adopted in this design. By embedding curvature compensation directly within the sensing front-end, the need for post-conversion digital calibration is eliminated, which is particularly advantageous for resource-constrained energy-harvesting nodes where computational overhead and memory footprint must be minimized [21,22]. Complementing this thermal sensing capability, the resistive interface achieves a dynamic

range of 109.2 dB in a fully dynamic dual-mode adjustable-gain configuration, surpassing the typical requirements for environmental monitoring applications. This wide dynamic range ensures reliable signal acquisition across varying sensor impedances without requiring external gain reconfiguration. The self-calibrating gain loop further simplifies the system architecture by autonomously adjusting to optimal operating points, thereby reducing design complexity and enabling seamless integration with low-power microcontroller units [23,24]. Recent advances in compact sensor interface design have demonstrated that aggressive area and power scaling can be achieved without sacrificing measurement fidelity, reinforcing the viability of the proposed approach for energy-autonomous operation. The small silicon footprint and low power consumption collectively position the front-end as a practical solution for deployment in distributed sensing networks. While these results compare favorably with prior art, direct benchmarking remains constrained by differences in process technology, supply voltage, and measurement conditions across reported implementations.

5.2. Limitations and Future Work

While the proposed front-end achieves competitive performance, several limitations delineate clear pathways for future enhancement, as summarized in the roadmap of Figure 5. The current implementation relies on a single fixed supply and lacks on-chip energy harvesting, meaning that autonomous operation still depends on an external source. Integrating a dedicated power management unit therefore constitutes the most immediate extension, and, as the figure indicates, this step naturally enables subsequent exploration of sub-threshold operation for further power reduction. A second constraint concerns thermal robustness: the present characterization spans a moderate temperature window, and extending it toward automotive-grade requirements would demand careful compensation of leakage and bias drift. Recent temperature-sensing architectures have demonstrated that tight accuracy over a wide range can be achieved without resorting to backend nonlinearity correction, suggesting that a similarly correction-free strategy could be embedded within the front-end to relax calibration overhead [8]. On the sensing side, the resistive interface could be reconfigured for capacitive transducers through relatively minor modifications, thereby broadening the range of detectable physical quantities. Such a transition would, however, require attention to charge-injection effects and to maintaining a wide dynamic range under varying excitation conditions, a challenge that adjustable-gain interface topologies are well positioned to address. Finally, ongoing efforts in low-power sensor readout continue to inform these directions, and the present work is intended to contribute to that broader trajectory. Collectively, these extensions would substantially widen the applicability of the front-end across diverse energy-harvesting IoT deployments [7,24]. Beyond hardware-level refinements, uncertainty-aware resource allocation and consensus-based termination, as introduced by Liu et al., offer a complementary perspective on balancing calibration effort against measurement confidence, particularly when multiple sensing modalities must share a limited energy budget in future multi-modal IoT nodes [25].

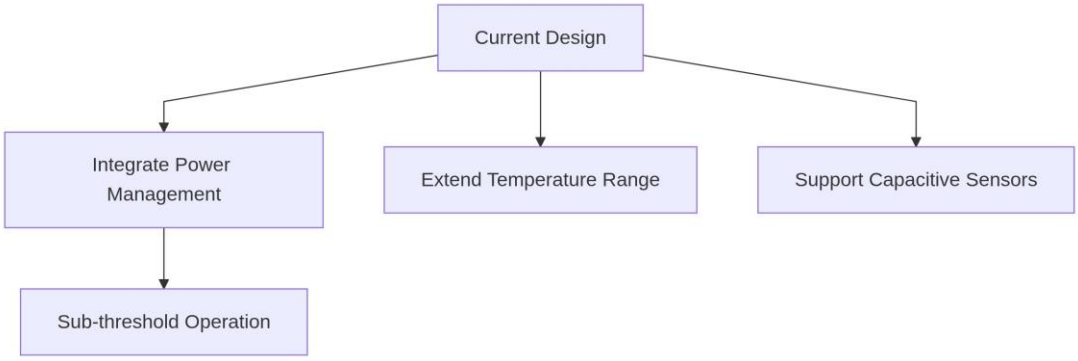


Figure 5. Roadmap for Future Enhancements

6. Conclusion

6.1. Summary of Contributions

This work presented a low-power analog front-end tailored for energy-harvesting Internet-of-Things sensor nodes, integrating three complementary capabilities within a compact silicon footprint. A temperature-sensing channel achieves ±0.25 C (3σ) inaccuracy from -40 C to 125 C without relying on backend nonlinearity correction, thereby eliminating costly digital calibration overhead. Complementing this, a fully dynamic dual-mode resistive interface delivers a 109.2 dB dynamic range, accommodating widely varying transducer impedances under harvested-power constraints. A self-calibrating gain mechanism further stabilizes signal acquisition against process and environmental drift. Collectively, these techniques reduce digital complexity and power consumption, yielding a prototype that dissipates only 3.5 μW while occupying 0.0251 mm^2, demonstrating a favorable balance among precision, dynamic range, and energy efficiency for autonomous sensing applications.

6.2. Final Remarks

The presented front-end validates that correction-free temperature sensing and wide-dynamic-range resistive interfacing can be co-integrated within a compact, low-power footprint, supporting self-powered operation. Extending this platform toward on-chip energy harvesting and broader operating ranges constitutes the primary direction for future investigation.

References

1. Y. Chi, H. Zhang, Z. Zheng, R. Liu, L. Qiao, and W. Cui, "Analog front-end circuit design for wireless sensor system-on-chip," in *Proc. IEEE 4th Inf. Technol., Netw., Electron. Autom. Control Conf. (ITNEC)*, vol. 1, Jun. 2020, pp. 38–42.
2. J. Fan, B. Zhao, and Y. Luo, "A 109.2 dB-dynamic-range fully dynamic dual-mode adjustable gain resistive sensor interface circuit," in *Proc. ICTA*, 2024.
3. X. Liu et al., "RF energy harvesting integrated circuits for low-power sensors: A review," *IEEE Sensors J.*, 2026.
4. H. Vishe, V. Wagh, and V. Vedak, "Adaptive mixed-signal front-ends for energy-harvesting battery-less sensors."
5. Z. Xin, Y. Tianqi, X. Wei, W. Shun, and X. Ma, "An ultra-low-power biopotential acquisition analog front-end chip for wearable devices," *Int. J. Circuit Theory Appl.*, 2026.
6. Q. Hong, "Optimization design of IoT sensor front-end circuit based on low power adaptive algorithm," in *Proc. Int. Conf. Intell. Commun. Netw. Comput. Techn. (ICICNCT)*, Sep. 2025, pp. 01–07.
7. A. Wattiez, "Design of an ultra-low-power always-on analog front-end for audio events detection in forests."
8. J. P. Shen, X. A. Wang, S. Liu, and J. F. Huang, "Ultra-low power analog front-end for passive UHF RFID tags," in *Proc. IET Int. Conf. Inf. Sci. Control Eng. (ICISCE)*, Stevenage, U.K., Dec. 2012, pp. 2–56.
9. J. Fan et al., "A 0.0251 mm^2 Temperature Sensor Achieving a ±0.25 °C (3σ) Inaccuracy From –40 °C to 125 °C Without Backend Nonlinearity Correction," *IEEE Trans. Circuits Syst. I, Reg. Papers*, 2026.
10. H. Lin et al., "A 2.1 μA 1.65 V-to-5V Supply 10ppm/°C Bandgap Reference with Source-Degenerated Multi-Sectional Curvature Compensation and CMOS-Voltage Reference Assisted Start-Up Circuit," in *Proc. ICTA*, 2025.
11. D. S. N. Rao, "A comprehensive survey on analog front-end circuits in digital converters with emphasis on biomedical sensor applications," *Int. J. Appl. Math.*, vol. 38, no. 2s, pp. 1151–1189, 2025.
12. W. X. Lian, "Integrated multiband front-end radio frequency energy harvesting system for low-power IoT devices," Doctoral dissertation, Univ. Malaya, Malaysia, 2023.
13. H. Hu, C. C. Lin, and S. Gupta, "A 197.1-μW wireless sensor SoC with an energy-efficient analog front-end and a harmonic injection-locked OOK TX," *IEEE Trans. Circuits Syst. I, Reg. Papers*, vol. 68, no. 6, pp. 2444–2456, 2021.
14. F. Yan and J. Liu, "Analog front-end input-impedance boosting techniques for bio-potential monitoring—A review," *IEEE Trans. Instrum. Meas.*, vol. 73, pp. 1–14, 2024.
15. Z. Zhu and W. Bai, "A 0.5-V 1.3-μW analog front-end CMOS circuit," *IEEE Trans. Circuits Syst. II, Exp. Briefs*, vol. 63, no. 6, pp. 523–527, 2016.
16. I. Akita, T. Okazawa, Y. Kurui, A. Fujimoto, and T. Asano, "A feedforward noise reduction technique in capacitive MEMS accelerometer analog front-end for ultra-low-power IoT applications," *IEEE J. Solid-State Circuits*, vol. 55, no. 6, pp. 1599–1609, 2019.
17. I. Kim, Y. A. Bhagat, J. Homer, and R. Lobo, "Multimodal analog front end for wearable bio-sensors," *IEEE Sensors J.*, vol. 16, no. 24, pp. 8784–8791, 2016.
18. A. Kosari, J. Breiholz, N. Liu, B. H. Calhoun, and D. D. Wentzloff, "A 0.5 V 68 nW ECG monitoring analog front-end for arrhythmia diagnosis," *J. Low Power Electron. Appl.*, vol. 8, no. 3, p. 27, 2018.

19. R. Olivieri and G. Ferri, "Recent advances in analog front-end architectures for ECG signal acquisition," *IEEE Sensors Rev.*, vol. 3, pp. 76–88, 2025.
20. W. Guo, W. Zhang, S. Wang, and R. Liu, "Efficient Test-Time Adaptation for Dynamic Distribution Shifts," 2026.
21. A. M. Elgani et al., "A clockless temperature-compensated nanowatt analog front-end for wake-up radios based on a band-pass envelope detector," *IEEE Trans. Circuits Syst. I, Reg. Papers*, vol. 67, no. 8, pp. 2612–2624, 2020.
22. D. Prasad and M. B. Elamien, "ECG analog front-end instrumentation for wearable cardiac monitoring: Architectures, signal-quality limits, and design trends," *IEEE Trans. Instrum. Meas.*, 2026.
23. Y. P. Hsu, "Analog front-end circuits for health monitoring applications," Rensselaer Polytechnic Institute, 2019.
24. J. Holleman, D. Yeager, R. Prasad, J. R. Smith, and B. Otis, "NeuralWISP: An energy-harvesting wireless neural interface with 1-m range," in *Proc. IEEE Biomed. Circuits Syst. Conf.*, Nov. 2008, pp. 37–40.
25. R. Liu, W. Guo, T. Liao, and X. Fang, "Uncertainty-Aware Adaptive Debate for Robust and Efficient Large Language Model Reasoning," 2026.

Disclaimer/Publisher's Note: The statements, opinions and data contained in all publications are solely those of the individual author(s) and contributor(s) and not of Publisher and/or the editor(s). Publisher and/or the editor(s) disclaim responsibility for any injury to people or property resulting from any ideas, methods, instructions or products referred to in the content.